

PROPAGATING DISTRIBUTIONS FOR SEGMENTATION OF BRAIN ATLAS

T. Riklin-Raviv, N. Sochen[‡], N. Kiryati, N. Ben-Zadok

S. Gefen, L. Bertand, J. Nissanov

School of Electrical Engineering
[‡]School of Mathematical Sciences
Tel-Aviv University*

Lab of Bioimaging and Anatomical Informatics
Department of Neurobiology and Anatomy
Drexel University College of Medicine[†]

ABSTRACT

We present a novel method for segmentation of anatomical structures in histological data. Segmentation is carried out slice-by-slice where the successful segmentation of one section provides a prior for the subsequent one. Intensities and spatial locations of the region of interest and the background are modeled by three-dimensional Gaussian mixtures. This information adaptively propagates across the sections. Segmentation is inferred by minimizing a cost functional that enforces the compatibility of the partitions with the corresponding models together with the alignment of the boundaries with the image gradients. The algorithm is demonstrated on histological images of mouse brain. The segmentation results compare well with manual segmentation.

Index Terms— Segmentation, Brain atlas, Level sets, Gaussian mixture model

1. INTRODUCTION

Automatic extraction of volumes of interest (VOIs) within experimental dataset of brain images can be facilitated by the availability of an atlas. The atlas consists of delineated and tagged anatomical structures of reference brain images. Usually, due to the high accuracy required from an atlas, segmentation is carried out manually by an expert. This manual segmentation is time consuming and laborious, therefore, automatic method for atlas segmentation is sought.

We address the problem of volumetric atlas segmentation based on a high resolution dataset in the presence of tight memory constraints. Segmentation is therefore carried out slice-by-slice where the successful segmentation of one section provides the initial conditions for the next one. Slices are sequentially partitioned into two inhomogeneous regions - the ROI (sliced anatomical structure of interest) and the background. The intensities and spatial locations of the regions are modeled by two distinct three dimensional Gaussian

mixtures. The GMM parameters adaptively propagate across slices, possibly in a bidirectional manner.

The foundation of the proposed method is the construction of a unified edge-based region-based segmentation functional. A key contribution is a region-based energy term that considers the probability density functions (PDFs) of the partitions. Since histological data is less noisy than the images obtained by other modalities, the magnitudes and directions of the image gradients are used to enhance the segmentation.

We use the level set framework [1] for segmentation, where the segmenting curve is the zero level of a level set function that evolves subject to some predefined constraints. Being parameterization-free, the level-set model allows automatic changes in the active contour topology. This feature has particular importance when the volume traced along the slices splits or merges.

Methods that use GMM for segmentation have been presented before, e.g. [2]. The works of [3, 4, 5] introduce a variational framework for image segmentation using the PDFs of the partitions. Slice-by-slice approaches for volumetric segmentation that use level-sets include [6, 5, 7]. Aykac et al [7] suggest an active contour algorithm for the segmentation of mouse spleen in micro-CT. However, their method, based on the piecewise constant image model of Chan and Vese is not suitable for segmentation of regions with heterogeneous intensities. Paragios [6] proposed a user guided model based on prior shape-knowledge for cardiac image analysis. Such shape-based approaches depend on the availability of reference shapes and credible alignment. Yet, since transformations between corresponding or consecutive slices are non-parametric they cannot be modeled reliably. Therefore, shape constraints, based on prior knowledge, are likely to deflect the contour evolution from the actual image data.

The proposed segmentation framework is capable of handling challenging segmentation tasks. This is accomplished by modeling the distribution functions of the image data and by imposing compatibility of the partitions to the model. The alignment of the ROI boundary with image gradients is constrained as well. The algorithm is demonstrated on images of histological atlas of mouse brain [8]. Results compare well with manual segmentation.

*The research at Tel-Aviv University was supported by the A.M.N. Foundation and by MUSCLE: a European Network of Excellence funded by the EC 6th Framework IST Programme.

[†]The research at Drexel University was supported by the NIH grant P20 MH62009

2. ALGORITHM DESCRIPTION

In the first part of this section the region-based and edge-based energy terms and associated gradient descent equations are presented. These energy terms are incorporated within a unified cost functional for single slice segmentation. The slice-by-slice segmentation framework is then described.

2.1. Level-set Approach

In this section we describe a level-set framework for image partitioning into two disjoint regions. Let $I: \Omega \rightarrow \mathbb{R}^+$ denote a gray level image, where $\Omega \subset \mathbb{R}^2$ is the image domain. Let ω^+ and ω^- be open subsets of Ω , denoting the region of interest (ROI) and the background, respectively. The optimal boundary $C \in \Omega$, $C = \partial\omega^+$ is obtained by minimizing a cost functional $E(C|I)$.

In this framework, we implicitly represent the curve C as the zero level of a level set function $\phi: \Omega \rightarrow \mathbb{R}$ at time t [1]:

$$C(t) = \{\mathbf{x} \in \Omega \mid \phi(\mathbf{x}, t) = 0\}. \quad (1)$$

The partition into two regions is done by using the Heaviside function of ϕ , [9]:

$$H(\phi(\mathbf{x})) = \begin{cases} 1 & \phi(\mathbf{x}) \geq 0 \\ 0 & \text{otherwise} \end{cases} \quad (2)$$

Note that for any arbitrary $f: \Omega \rightarrow \mathbb{R}$

$$\int_{\mathbf{x} \in \omega^\pm} f(\mathbf{x}) d\mathbf{x} = \int_{\mathbf{x} \in \Omega} f(\mathbf{x}) H(\pm\phi(\mathbf{x})) d\mathbf{x}.$$

2.2. Region-based term

Region based segmentation approaches assumes homogeneity of semantic regions within the image, usually in terms of pixels intensities [9]. The proposed framework extends the concept of region homogeneity to include probability density functions of the pixels feature vectors. This allows to extract ROIs with heterogeneous intensities.

Let $G(\mathbf{x}) = (x, y, I(x, y))$ be a vector representation of the pixel $(x, y) \in \Omega$. We assume that $G(\mathbf{x})$ are drawn from two distinct probability density functions, p^+ if $\mathbf{x} \in \omega^+$ and p^- otherwise. Specifically, p^+ and p^- are Gaussian mixture models of $(\omega^+, I(\omega^+))$ and $(\omega^-, I(\omega^-))$, respectively. Assuming an independent and identically distributed conditional PDF, we get:

$$P(G(\mathbf{x})|\phi) = \prod_{\mathbf{x} \in \omega^+} p^+(\mathbf{x}) \prod_{\mathbf{x} \in \omega^-} p^-(\mathbf{x}). \quad (3)$$

hence,

$$\log P(G(\mathbf{x})|\phi) = \int_{\mathbf{x} \in \omega^+} \log p^+(\mathbf{x}) d\mathbf{x} + \int_{\mathbf{x} \in \omega^-} \log p^-(\mathbf{x}) d\mathbf{x}. \quad (4)$$

The region based (RB) energy term to be minimized thus takes the form [3, 4]:

$$E_{\text{RB}} = - \int_{\mathbf{x} \in \Omega} [\log p^+(\mathbf{x}) H(\phi) + \log p^-(\mathbf{x}) H(-\phi)] d\mathbf{x}. \quad (5)$$

In the proposed framework, the PDFs p^+ and p^- are multivariate Gaussian densities

$$p^+(\mathbf{x}|\theta^+) = \sum_{i=1}^{N^+} w_i^+ \frac{\exp\{-\frac{1}{2}(\mathbf{x} - \mu_i^+)^T \Sigma_i^{+^{-1}} (\mathbf{x} - \mu_i^+)\}}{\sqrt{(2\pi)^3 |\Sigma_i^+|}} \quad (6)$$

$$p^-(\mathbf{x}|\theta^-) = \sum_{i=1}^{N^-} w_i^- \frac{\exp\{-\frac{1}{2}(\mathbf{x} - \mu_i^-)^T \Sigma_i^{-^{-1}} (\mathbf{x} - \mu_i^-)\}}{\sqrt{(2\pi)^3 |\Sigma_i^-|}} \quad (7)$$

where, $\theta^\pm = \{w_i^\pm, \mu_i^\pm, \Sigma_i^\pm\}_{j=1}^{N^\pm}$ are the GMM parameters.

The gradient descent equation associated with E_{RB} is:

$$\phi_t^{\text{RB}} = \delta(\phi) [-\log p^+(\mathbf{x}) + \log p^-(\mathbf{x})], \quad (8)$$

where δ is the derivative of the Heaviside function H . The parameters θ^+ and θ^- are first estimated given the segmentation of the predecessor slice and then alternately updated with the evolution of ϕ . We use the EM technique [10] to estimate the GMM parameters.

2.3. Smoothness and Edge based terms

Contour smoothness is imposed by minimizing its length $|C| = \int_0^1 ds$, where s is the curve length parameter. The length term in a level set formulation takes the form:

$$E_{\text{LEN}} = \int_{\Omega} |\nabla H(\phi(\mathbf{x}))| d\mathbf{x}. \quad (9)$$

Since histological images are less noisy than the data obtained by other modalities we can employ the image gradients as well. Next, we describe two edge-based terms that are incorporated within the proposed segmentation functional.

2.3.1. Geodesic active contour term

Following [11, 12], the inverse edge indicator function is defined by;

$$g_{\text{GAC}}(\mathbf{x}) = 1/(1 + |\nabla I|^2), \quad (10)$$

where ∇I denote the vector field of the image gradients. The geodesic active contour functional (GAC) integrates the inverse edge indicator along the curve.

$$E_{\text{GAC}} = \int_{\Omega} g_{\text{GAC}}(\mathbf{x}) |\nabla H(\phi(\mathbf{x}))| d\mathbf{x}. \quad (11)$$

This functional is minimized when the zero level of ϕ is aligned with the local maxima of the image gradients. The evolution of ϕ is determined by:

$$\phi_t^{\text{GAC}} = \delta(\phi) \text{div} \left(g_{\text{GAC}}(\mathbf{x}) \frac{\nabla \phi}{|\nabla \phi|} \right). \quad (12)$$

2.3.2. Edge alignment term

To enhance the segmentation we impose the normal direction of the level set $\vec{n} = \frac{\nabla\phi}{|\nabla\phi|}$ to align with the image gradients direction [13, 14]. This is obtained by minimizing the robust alignment (RA) energy term:

$$E_{RA} = - \int_{\Omega} |\langle \nabla I, \frac{\nabla\phi}{|\nabla\phi|} \rangle| |\nabla H(\phi)| dx. \quad (13)$$

The associated gradient descent equation is:

$$\phi_t^{RA} = \delta(\phi) \text{sign}(\langle \nabla\phi, \nabla I \rangle) \Delta I, \quad (14)$$

where Δ is the divergence operator.

2.4. Unified cost functional

A unified region-based, edge-based cost functional takes the following form:

$$E(\phi) = W^{RB} E_{RB}(\phi) + W^{GAC} E_{GAC}(\phi) + W^{RA} E_{RA}(\phi), \quad (15)$$

according to equations (5), (11) and (13) for E_{RB} , E_{GAC} and E_{RA} respectively¹. The evolution of the level-set functions ϕ at each iteration is determined by $\phi(t + \Delta t) = \phi(t) + \phi_t$. The associated gradient descent equations ϕ_t are derived using the first variation of the functional (15) above,

$$\phi_t(\phi) = W^{RB}(t) \phi_t^{RB} + W^{GAC}(t) \phi_t^{GAC} + W^{RA}(t) \phi_t^{RA}, \quad (16)$$

The weight terms $W^{TERM}(t)$ in (15,16) are adaptively changing scalars. Their determination is explained in [15].

2.5. Slice by Slice Segmentation

The segmentation algorithm proposed in the previous section is applied to images of consecutive brain slices. Given a sequence of images $\{\dots, I_{s-1}, I_s, I_{s+1}, \dots\}$, the final estimates of either $(\phi_{s-1}, \theta_{s-1})$ or $(\phi_{s+1}, \theta_{s+1})$ are used to initialize (ϕ_s, θ_s) . The level-set function ϕ_s and the GMM parameters θ_s are updated alternately. We assume that the segmentation of few sparsely sampled slices is done manually. Once the segmentation is known the PDF parameters can be computed accordingly. This information then propagates in both directions. In the post-processing phase, the delineating contours of the image sequence are stacked together to generate a model of the VOI.

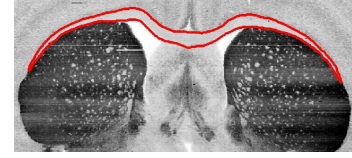
3. EXPERIMENTS

The images utilized in this study are sampled coronal views of a 3D brain atlas of a C57BL/6J mouse. The atlas was generated from consecutive 17.9 μ m thick horizontal sections of

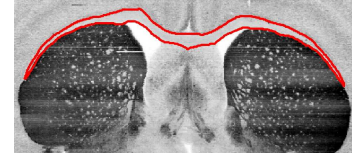
¹One may replace the edge terms (11) and (13) with the length term (9) when the data is noisy and the image gradients are not reliable.



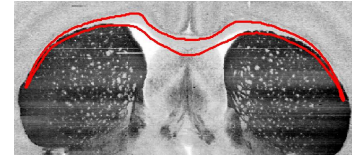
(a) slice #509



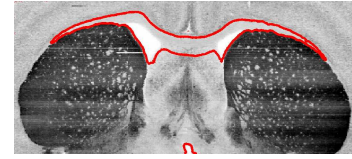
(b) slice #509: Segmentation with the proposed algorithm



(c) slice #509: Manual Segmentation



(d) slice #509 with the contour (red) of slice #500

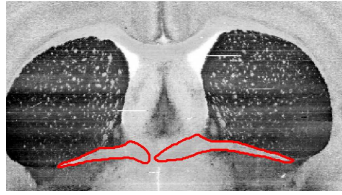


(e) slice #509: Segmentation with Chan-Vese model

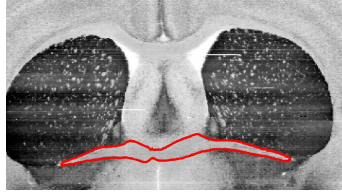
Fig. 1. Segmentation of the last slice of 10 slices sequence.

a freshly frozen adult male brain [16]. The sections were stained for acetylcholinesterase and imaged to yield a pixel pitch of $8\mu\text{m}$. The volume was reconstructed based on the block face images [17, 18]. It was then downsampled to yield an isotropic $17.9\mu\text{m}$ /voxel atlas.

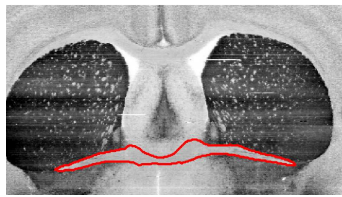
Figure 1a-b exemplify segmentation of the last slice in a sequence of 10 consecutive slices. The manual segmentation, Figure 1c, is displayed for a comparison. Segmentation of the complete sequence is accessible online at [19]. Mixtures of 4 and 8 Gaussian have been used to model the ROI and the background, respectively, based on the manual segmentation of the first slice (# 500). Figure 1d demonstrates the gradual change of the ROI by displaying the image of slice #509 together with the ROI contour (red) of slice #500. To demonstrate the advantage of the proposed algorithm we present the unsuccessful segmentation, Figure 1e, obtained using a region-based term that is established on a piecewise constant image model [9] as used in [7]. A quantitative comparison



(a) slice #320: Manual Segmentation



(b) slice #321: Segmentation with the proposed algorithm



(c) slice #321: Manual Segmentation

Fig. 2. Successful segmentation when two ROIs merge

between the manual segmentation and the segmentation obtained by the proposed algorithm is shown in Table 1.

Figure 2b demonstrates successful segmentation when two disjoint ROIs that belong to the same structure merge. Manual segmentation is shown for a comparison in Figure 2c.

| 501 | 502 | 503 | 504 | 505 | 506 | 507 | 508 | 509 |
|-----|-----|------|------|------|------|------|------|------|
| .87 | .93 | 1.03 | 1.31 | 1.41 | 1.48 | 1.73 | 1.93 | 2.14 |

Table 1. The percentage of pixels with dissimilar labeling with respect to the total number of pixels for slices 501 – 509

4. SUMMARY

A method for slice-by-slice segmentation of mouse brain histological data is presented. The information on the spatial and intensity distributions of the region of interest is propagated along the slices. The ROI in each slice is extracted by minimizing a unified region-based edge-based functional. Promising segmentation results on challenging data are shown.

5. REFERENCES

[1] S. Osher and J.A. Sethian, “Fronts propagating with curvature-dependent speed: Algorithms based on Hamilton-Jacobi formulations,” *J of Comp Phys*, vol. 79, pp. 12–49, 1988.

[2] A. Shahar and H. Greenspan, “Probabilistic spatial-temporal segmentation of multiple sclerosis lesions,” *ISBI*, vol. 1, no. 15–18, pp. 440–443, April 2004.

[3] S.C. Zhu and A.L. Yuille, “Region competition: Unifying snakes, region growing, and bayes/MDL for multiband image segmentation,” *PAMI*, vol. 18, no. 9, pp. 884–900, 1996.

[4] N. Paragios and R. Deriche, “Geodesic active regions: A new paradigm to deal with frame partition problems in computer vision,” *JVCIR*, vol. 13, pp. 249–268, 2002.

[5] N. Paragios, “Variational methods and partial differential equations in cardiac image analysis,” *ISBI*, vol. 1, no. 15–18, pp. 17–20, 2004.

[6] N. Paragios, “A variational approach for the segmentation of the left ventricle in cardiac image analysis,” *IJCV*, vol. 50, pp. 345–362, 2002.

[7] Aykac et al, “3d segmentation of mouse spleen in micro-ct via active contours,” *IEEE Nuclear Science Symposium Conference Record*, vol. 3, pp. 1542–1545, 2005.

[8] C. Gustafson, O. Tretiak, L. Bertrand, and Y. Nissanov, “Design and implementation of software for assembly and browsing of 3d brain atlases,” *Computer Methods and Programs in Biomedicine*, vol. 74, pp. 53–61, 2004.

[9] T.F. Chan and L.A. Vese, “Active contours without edges,” *IP*, vol. 10, no. 2, pp. 266–277, 2001.

[10] Dempster et al, “Maximum likelihood from incomplete data via the EM algorithm,” *J. Royal Stat. Soc. Series B*, vol. 39, no. 1, pp. 1–38, 1977.

[11] S. Kichenassamy, A. Kumar, P.J. Olver, A. Tannenbaum, and A. Yezzi, “Gradient flows and geometric active contour models,” in *ICCV*, 1995, pp. 810–815.

[12] V. Caselles, R. Kimmel, and G. Sapiro, “Geodesic active contours,” *IJCV*, vol. 22, no. 1, pp. 61–79, 1997.

[13] A. Vasilevskiy and K. Siddiqi, “Flux maximizing geometric flows,” in *ICCV*, 2001, pp. 149–154.

[14] R. Kimmel and A.M. Bruckstein, “Regularized laplacian zero crossings as optimal edge integrators,” *IJCV*, vol. 53, no. 3, pp. 225–243, 2003.

[15] T. Riklin-Raviv, N. Kiryati, and N. Sochen, “Prior-based segmentation and shape registration in the presence of projective distortion,” *IJCV*, vol. 72, no. 3, 2007.

[16] J. Nissanov and O. Bertrand, L. Tretiak, “Cryosectioning distortion reduction using tape support,” *Microsc Res Tech*, vol. 53, pp. 239–240, 2001.

[17] Woods et al, “Automated image registration: 2. intersubject validation of linear and nonlinear models,” *J Comput Assist Tomogr*, vol. 22, pp. 153–165, 1998.

[18] Rosen et al, “Informatics center for mouse genomics: The dissection of complex traits of the nervous system,” *Neuroinformatics*, vol. 1, pp. 327–342, 2003.

[19] T. Riklin-Raviv, “Brain segmentation examples,” <http://www.eng.tau.ac.il/~tammy/BrainResults.htm>.